Steel and Composite Structures, *Vol. 19, No. 3 (2015) 601-614*
DOI: http://dx.doi.org/10.12989/scs.2015.19.3.601

Investigating the fatigue failure characteristics of A283 Grade C steel using magnetic flux detection

A. Arifin [a], W.Z.W. Jusoh [*], S. Abdullah [b], N. Jamaluddin and A.K. Ariffin

Department of Mechanical & Materials Engineering, Faculty of Engineering and Built Enviroments, Universiti Kebangsaan Malaysia, 43600 UKM Bangi, Selangor, Malaysia

(*Received December 26, 2014, Revised July 01, 2014, Accepted February 04, 2015*)

Abstract. The Metal Magnetic Memory (MMM) method is a non-destructive testing method based on an analysis of the self-magnetic leakage field distribution on the surface of a component. It is used for determining the stress concentration zones or any irregularities on the surface or inside the components fabricated from ferrous-based materials. Thus, this paper presents the MMM signal behaviour due to the application of fatigue loading. A series of MMM data measurements were performed to obtain the magnetic leakage signal characteristics at the elastic, pre-crack and crack propagation regions that might be caused by residual stresses when cyclic loadings were applied onto the A283 Grade C steel specimens. It was found that the MMM method was able to detect the defects that occurred in the specimens. In addition, a justification of the Self Magnetic Flux Leakage patterns is discussed for demonstrating the effectiveness of this method in assessing the A283 Grade C steel under cyclic loadings.

Keywords: fatigue; stress concentration; steel; metal magnetic memory; crack propagation

1. Introduction

Stress concentration (SC) occurs when a metal component or material under repeated work load and have high localized stresses. It is important to know where the stress concentration zones (SCZ) are so that the component can be evaluated before it fails (Dong *et al*. 2010). The failure of a component in structures or machines could lead to accidents and casualties. Thus, by preventing this from occurring, catastrophic accidents and even death can be avoided. SCZ have a high possibility of causing a component to undergo plastic deformation, to crack and to lead to the failure of the component after repeated loads. Metal magnetic memory (MMM) technology is a recent non-destructive testing (NDT) that was initially introduced by a Russian scholar in the field of power engineering (Dubov 1995). The MMM method can be effectively used in many industries in order to determine the SCZ with the localised detection of residual magnetism in any ferrous-based materials. When work load is imposed on ferromagnetic materials, fabrication and the effect of the earth's magnetic field tend to change the magnetic properties of the material itself.

∗Corresponding author, M.Sc. Student, E-mail: zulhelmi@eng.ukm.my
[a] E-mail: azli@eng.ukm.my
[b] E-mail: shahrum@eng.ukm.my

http://www.techno-press.org/?journal=scs&subpage=8 ISSN: 1229-9367 (Print), 1598-6233 (Online)

After the load is applied to the materials, the microstructure changes from its original state, and then it changes the magnetic characteristics of the material. These kind of characteristic forms are called Self Magnetic Flux Leakage (SMFL) (Li and Xu 2012). The MMM has attracted great interest in academia and in industries and can be used in various engineering fields (Dubov and Kolokolnikov 2013, Yang *et al*. 2013). It has risen quickly in the area of non-destructive testing for many applications, particularly in oil and gas industries (Wang *et al*. 2012).

The SMFL components are the main criteria for detecting the SCZ and for finding the highest potential defect location due to various loadings. The tangential component $H_p(x)$ and the normal component $H_p(y)$ of the SMFL signals are measured on the surface of the component. When the maximum SCZ occur, $H_p(x)$ has the maximum value and it gives the $H_p(y)$ effect to change the polarity (Wang *et al*. 2010a). Several applications have been known to use the MMM method for diagnosing gas and oil pipelines, rails, turbine wheels, pressure vessels and lots more (Dubov 2006, Wang *et al*. 2012). The advantages of the MMM method are that it has a very fast scanning speed, it is easy to operate and it does not require any removal of surface coating or insulation for up to 50 mm in thickness (Wang *et al*. 2012). Compared to other NDT method such as ultrasonic testing, acoustic emission, Eddy Current testing, etc., the sole disadvantage of MMM is only can be used for ferromagnetic material only.

Many research works have shown (Li *et al*. 2010, Wang *et al*. 2012, Xing *et al*. 2010, Yuan and Zhang 2011, Zhang *et al*. 2012) that the SMLF signal tends to effectively detect micro-cracks and SCZ. It denotes that this method is capable of detecting any irregularity towards fatigue failure behaviour and its damage mechanism. However, certain things are still unclear with regard to this method, such as the lack of a physical model of relations between the SMFL signals with defects and the lack of quantitative criteria in defect features (Wang *et al*. 2012, 2010b). Furthermore, laboratory tests have been carried out and the MMM is used to evaluate fatigue damage in train axles plus in operations on railway systems, and also to try and predict the residual life of older machines (Leng *et al*. 2009).

This paper presents an experimental research on the Metal Magnetic Memory method under fatigue loading. Although researches have been carried out on this new technology (Li *et al*. 2010, Wang *et al*. 2012, Xing *et al*. 2010, Yuan and Zhang 2011), it is still necessary to conduct further researches so as to attain a better understanding of this method and to find better correlation between MMM at tensile, fatigue, creep, torsion etc. Furthermore, there is still a lack of physical criteria and quantitative results for the MMM method (Dong *et al*. 2009, 2012). The focus of this paper is on finding the behaviour of the Metal Magnetic Memory signal patterns due to fatigue and its significance in detecting failure. Additionally, it presents the relationship between Metal Magnetic Memory signals in elastic, pre-crack and crack growth regions of A283 Grade C steel. Also, in-depth observations have been made during crack growth propagation. Moreover, this is the first authors research to correlate the MMM and fatigue crack at 1 mm interval during crack growth propagation for A283 Grade C Steel. Thus, MMM characteristics at crack propagation during fatigue loading can be known. It presumes that the gradient of H_p will increase during the crack growth.

2. Theoretical background of the metal magnetic memory

The loads applied to ferromagnetic materials tend to change the dimensions of the materials in a microstructure scale. The loads also cause the magnetic domain to change from its original condition (Lindgren and Lepistö 2001). This phenomenon is called the magneto-mechanical effect (Jiles 1998), which is based on the magneto-elasticity and magneto-mechanical characteristics of the materials. The magnetic domain will dislocate and be irreversibly reoriented, while the ferromagnetic components are in operation and are loaded. As a result, in the dislocation concentration region, the self-leakage magnetic field will be visible at that moment. The irreversible transformation of this magnetic state will not only be preserved but will also coincide with the greatest stress following the dissolution of the load.

Due to stresses and the magnetic charge density of the local earth magnetic field existing on the surface of ferromagnetic materials, (Wang *et al*. 2010b) developed a linear charge density model for the SMLF in the existing near-crack area of which the differential components, *dH* of the self-magnetic field can be expressed in Eqs. (1) and (2), where ρ is the magnetic charge density, μ_0 is the magnetic permeability in the air, b is width of local distribution dislocation on material surface, l' and l are length at the right and left axis values on the surface of the materials.

$$\left.\begin{array}{c} dH_{1x} = \dfrac{\rho_{\max}\left(b + \dfrac{l}{b}\right) dl}{2\pi\mu_0[(x-l)^2 + y^2]} \cdot (x-l) \\ l \in [-b, 0] \\ dH_{1y} = \dfrac{\rho_{\max}\left(b + \dfrac{l}{b}\right) dl}{2\pi\mu_0[(x-l)^2 + y^2]} \cdot y \end{array}\right\} \tag{1}$$

$$\left.\begin{array}{c} dH_{2x} = \dfrac{\rho_{\max}\left(b + \dfrac{l'}{b}\right) dl'}{2\pi\mu_0[(x-l')^2 + y^2]} \cdot (x-l') \\ l' \in [0, b] \\ dH_{2y} = \dfrac{\rho_{\max}\left(b + \dfrac{l'}{b}\right) dl'}{2\pi\mu_0[(x-l')^2 + y^2]} \cdot y \end{array}\right\} \tag{2}$$

The total magnetic field leaked, *H* can be obtained by using the integer as in Eqs. (3) and (4).

$$H_{p(x)} = \int_{-b}^{0} dH_{1x} + \int_{0}^{b} dH_{2x} \tag{3}$$

$$H_{p(y)} = \int_{-b}^{0} dH_{1y} + \int_{0}^{b} dH_{2y} \tag{4}$$

The mathematical modelling of the damaged parameter of the plastic strain energy is as in Eq. (5).

$$D = 1 - \frac{\Delta S_0}{\Delta S_N} \tag{5}$$

(Changliang *et al*. 2010) explained it as the internal damage changes to the material and their impact on the mechanical effects using the damaged parameter as an internal state parameter. Where, ΔS_0 expresses the area of the initial stress-strain curve with the stress coordinate enclosed when there is no damage. Also, ΔS_N expresses the area of the stress-strain curve with the stress coordinate enclosed after N times of fatigue cycles. ΔH_{SN} is defined as shown in Eq. (6).

$$\Delta H_{SN} = \int_{x0}^{x1} \left| Hp(y)_{avgN} - Hp(y)_{avg\,0} \right| dx \tag{6}$$

Hence, the damaged parameter with the magnetic characteristic can be defined as in Eq. (7).

$$D = 1 - \frac{\Delta H_1}{\Delta H_{SN}} \tag{7}$$

3. Experimental method

The chosen specimen for the tests was fabricated from the A283 Grade C steel plate, which is commonly used in the construction of vessels and also in structural applications. Its mechanical properties and chemical composition are given in Tables 1 and 2 (C33 2004). The specimen used for the experimental procedure was designed according to the ASTM: E647 (International and Materials 2004), as shown in its geometry in Fig. 1, and the specimen thickness are 3 mm. The fatigue tests were then conducted using an INSTRON 8801 100 kN servo-hydraulic machine. The image of this machine is shown in Fig. 2. A tension-tension fatigue test with a testing frequency of 10 Hz was selected, and stress at 150 MPa was applied during the test in order to observe the stable crack growth propagation. These load and frequency was chosen as according as to our previous work, it was found that the strain and frequency greater than 6 kN and 20 KH will lead to unstable crack growth. As a result, it is complicate to achieve correlation between SMFL and crack. In addition, the SMFL data or response signals were captured using a special scanner containing two sensors, as exhibited in Fig. 3. In addition, the distance between sensor 1 and sensor 2 was

Table 1 Mechanical properties of A283 Grade C steel

Ultimate tensile strength	Yield tensile strength	Elongation	Bulk modulus	Shear modulus
380-485 Mpa	205 MPa	25%	140 GPa	80 GPa

Table 2 Chemical composition (wt %) of A283 Grade C steel

Carbon, C	Copper, Cu	Iron, Fe	Manganese, Mn	Phosphorus, P	Silicon, Si	Sulfur, S
0.24	>= 0.20	98.00	0.90	0.04	0.04	0.05

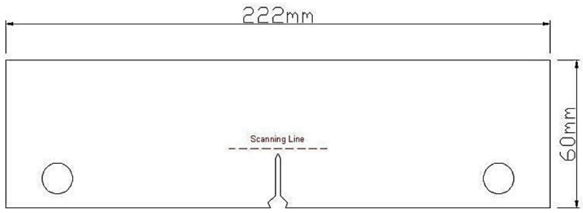

Fig. 1 Geometry (dimensions in mm) of notched fatigue specimens and scanning line of MMM signals

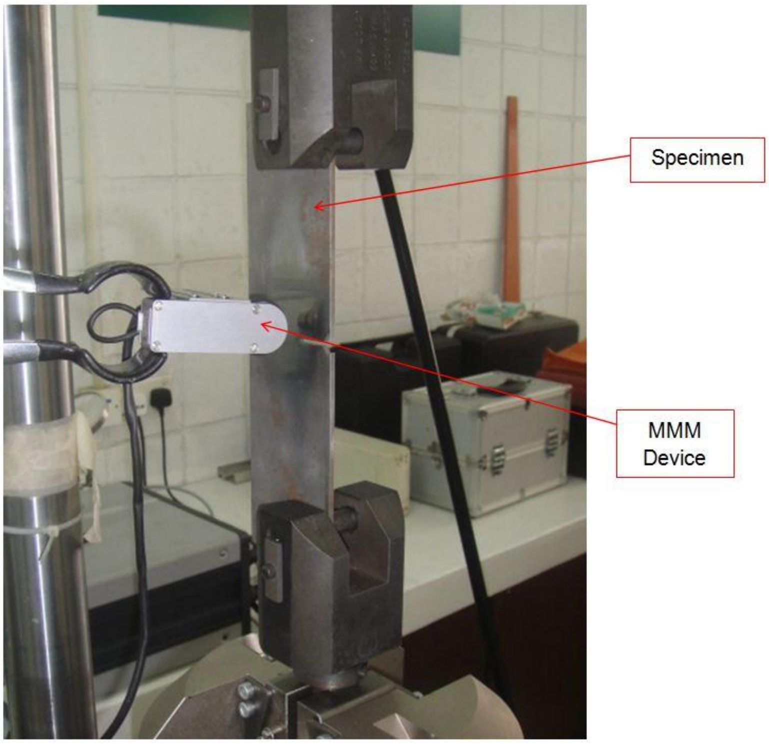

Fig. 2 The servo-hydraulic machine with specimen attached

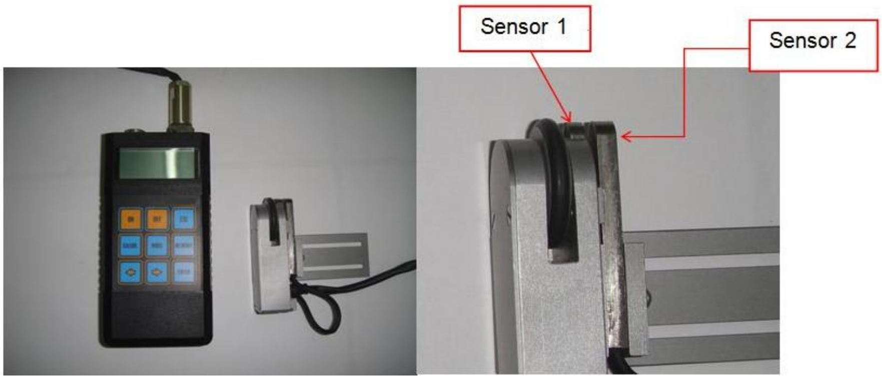

Fig. 3 The MMM scanning device

10 mm, also, the spacing from the surface of the specimen to sensors surface is 2 mm or identified as lift off value (Wang *et al*. 2010b). Accordingly, the EUROMAX PB4161 microscope was used for detecting the beginning of crack propagation on the specimen surface. A scanning line with a length of 40 mm was made to be vertical to the crack starter notch centre so that the data taken would go through the SCZ and the normal zone, and the line was 2 mm from crack starter notch to prevent the SMFL device from detecting the notch only. The specimen was scanned at the machine during the experiment in order to obtain the SMFL signal. Also, the fatigue test was paused for a while at predetermined cycles during the SMFL scanning on the surface in order to increase the variety and comparability of the data.

4. Results and discussion

4.1 Observation in the elastic region

The distributions of the SMFL for sensor 1 are shown in Fig. 4. The SMFL is represented by the early cycles in the fatigue test, which is categorised in an elastic region of the chosen steel material. Hp-1 to Hp-11 in Fig. 4 emblematized H_p signal at certain cycles ranging from 0 cycles to 4500 cycles as shown as in Cycles row in Table 3. It is also shown that the scanning line, L_x was 40 mm and the location of the crack starter notch and the occurrence of SCZ were at the 20 mm mark. The H_p increased in the middle of the elastic region, but the values started to decrease to -24 A/mm at 4,500 cycles, as shown in the detailed results in Table 3. This phenomenon occurred because at the beginning of the fatigue test the changes in the microstructure of the material were small due to loading (Changliang *et al*. 2010). Thus, the magnetic values were higher. However, after 1,600 cycles until 4,500 cycles it was observed that the H_p value was decreasing, the simple explanation being that the microstructures at these cycles were changing rapidly. Furthermore, this phenomenon clearly shown in Fig. 5. Also, like all ferromagnetic materials in the early stages of fatigue, the specimen was in the elastic deformation stage with few dislocations in its microstructure due to fatigue loading, as shown by the decreasing value of the H_p.

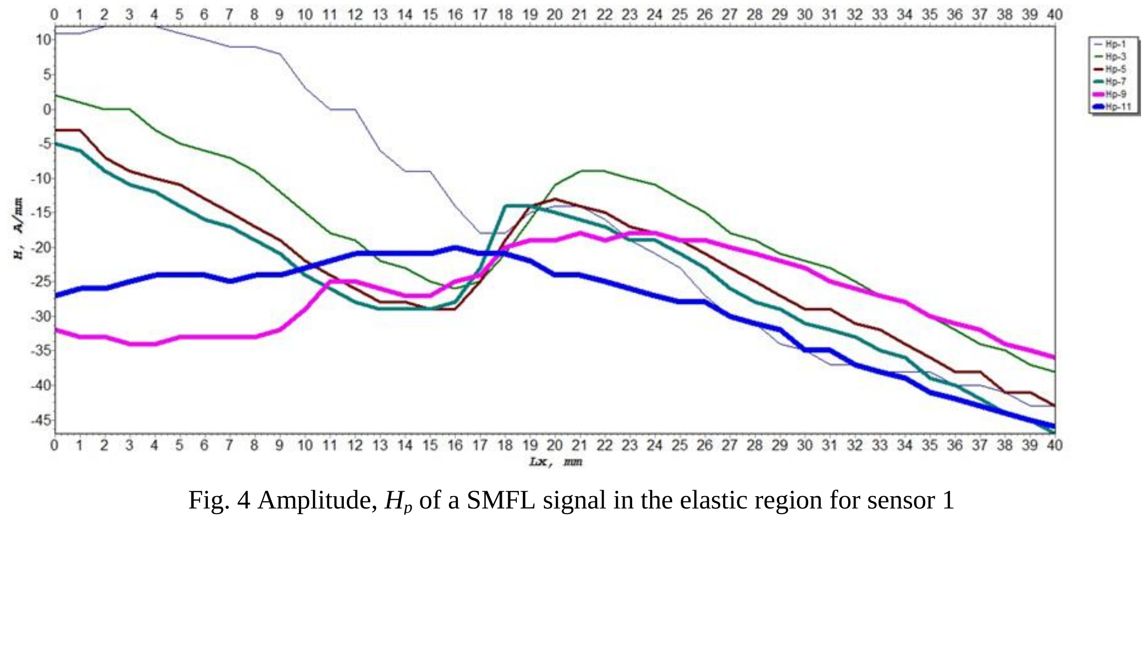

Fig. 4 Amplitude, H_p of a SMFL signal in the elastic region for sensor 1

Table 3 H_p values in the elastic region for sensor 1

Cycles	0	800	1,600	2,400	3,300	4,500
H_p value at SCZ , A/mm	-14	-11	-13	-15	-19	-24

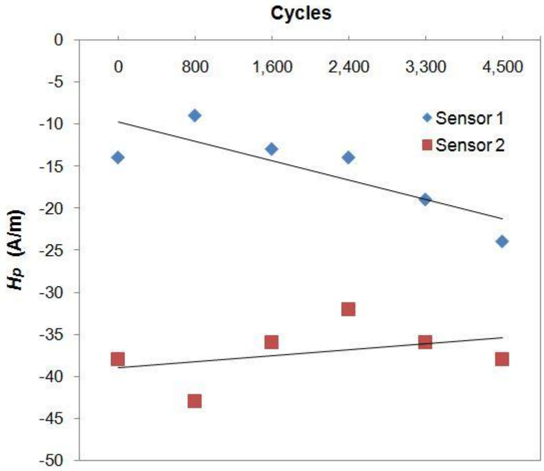

Fig. 5 Amplitude, H_p of a SMFL signal in the elastic region at crack starter notch

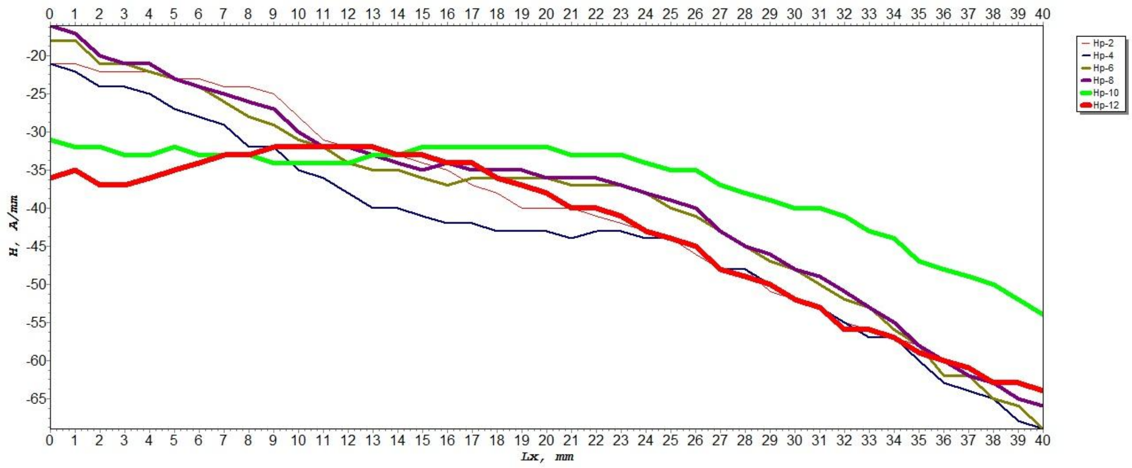

Fig. 6 Amplitude, H_p of a SMFL signal in the elastic region for sensor 2

Table 4 H_p values in the elastic region for sensor 2

Cycles	0	800	1,600	2,400	3,300	4,500
H_p value at SCZ, A/mm	-40	-43	-36	-36	-32	-38

Besides that, it can be seen that at L_x from 0 mm to 20 mm, the patterns of the H_p were changing randomly, but after 20 mm the patterns were the same and became more stable. This was because the loads were distributed equally after the length of the L_x at 20 mm.

The H_p value for sensor 2 at the crack starter notch is shown at a range from -43 A/mm to -32 A/mm as in Figs. 5, 6 and Table 4. Furthermore, Hp-2 to Hp-12 in Fig. 7 emblematized H_p signal at certain cycles ranging from 0 cycles to 4500 cycles as shown as in Cycles row in Table 4. Also, it can be observed that the values of these changing patterns were quite similar to the H_p value of sensor 1. However, it was less than the H_p values for sensor 1 ranging from -11 A/mm to -24 A/mm. The length from sensor 2 to the crack starter notch was 12 mm, thus indicating that the strength of the SMFL was weak due to the long distance from the SCZ.

4.2 Observation in the pre-crack region

The SMFL in this sub chapter is represented by the cycles just before crack occurred in the fatigue test, which is categorised in pre-crack region of the chosen steel material. The patterns of the SMFL distributions for sensors 1 and 2 were similar, but their values were different due to the small range of fatigue cycles. Fig. 7 and Table 5 represent the H_p values for sensor 1 and sensor 2; the same is also shown in the same graph and table. The H_p values range for sensor 1 was found to be between -19 A/mm to -24 A/mm, and for sensor 2 from -31 A/mm to -35 A/mm. Furthermore, Hp-1 to Hp-10 in Fig. 7 emblematized H_p signal at certain cycles ranging from 6100 cycles to 6900 cycles as shown as in Cycles row in Table 5.The small range of H_p occurred because the SMFL data were taken at cycles 6,100 to 6,900, which was just before the specimen began to

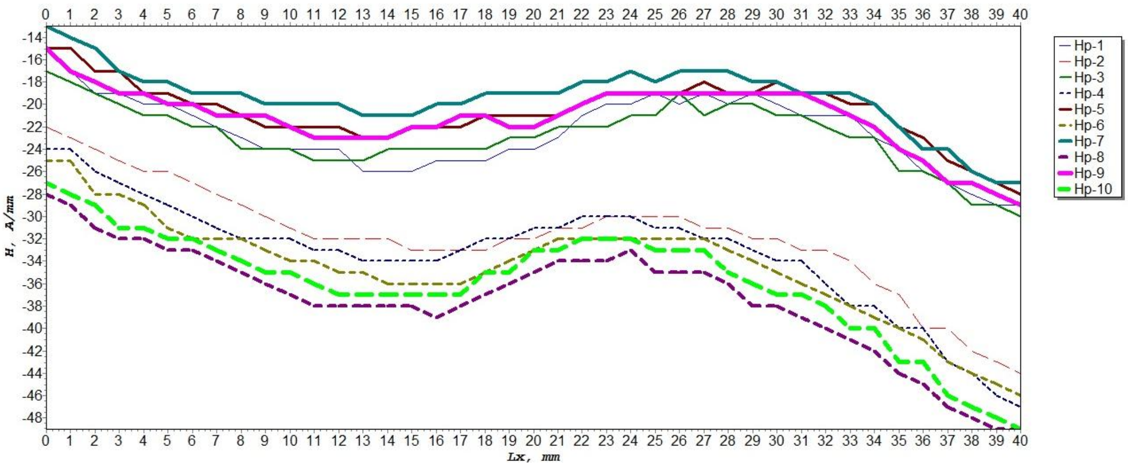

Fig. 7 Amplitude, H_p of SMLF signals in the pre-crack region

Table 5 H_p values in the pre-crack region

Cycles	6,100		6,300		6,500		6,700		6,900	
Sensor number	1	2	1	2	1	2	1	2	1	2
H_p value at SCZ, A/mm	-24	-32	-23	-31	-21	-33	-19	-35	-22	-33

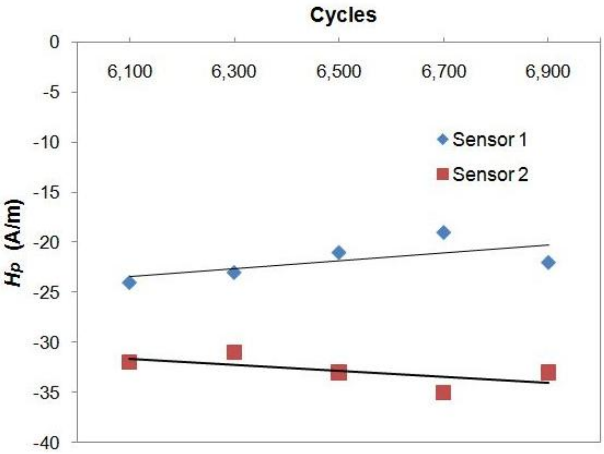

Fig. 8 Amplitude, H_p of a SMFL signal in the pre-crack region at crack starter notch

crack at 7,800 cycles. This state happened because the small increment of fatigue cycles tended to change only a small H_p value. Furthermore, it was confirm by small variation of H_p value at crack starter notch as shown in Fig. 8. However, obviously different patterns of the SMFL were shown between the pre-crack region and the elastic region because more dislocation occurred in the pre-crack region.

4.3 Observation in the crack propagation region

The SMFL in this sub chapter is represented by the cycles at crack propagation occurred in the fatigue test, which is categorised in crack propagation region of the chosen steel material. The final phase for this study was the SMFL characterisation of the crack propagation region (Fig. 9), which was the crack propagation starting from 7,800 cycles (Fig. 11) to the end of the test, which was at

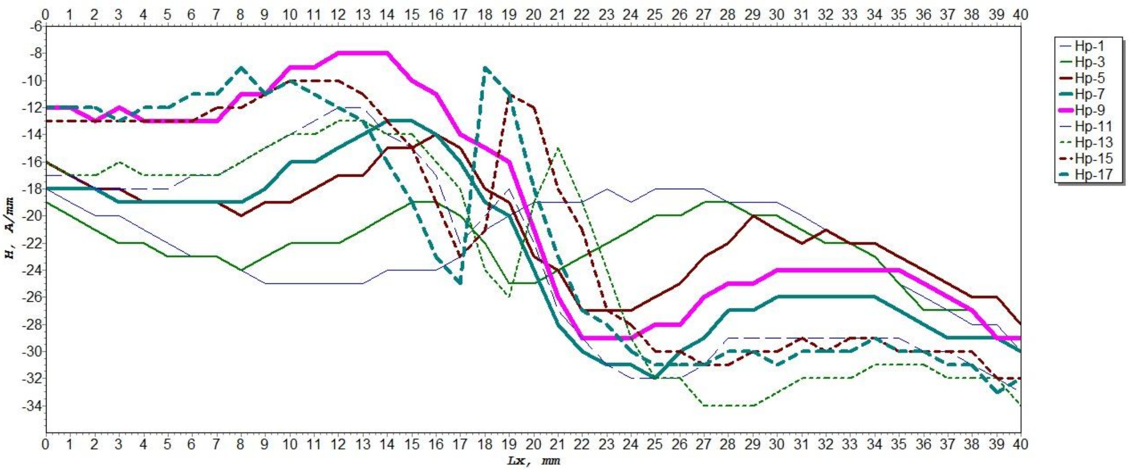

Fig. 9 Amplitude, H_p of SMFL signals in the crack propagation region for sensor 1

40,000 cycles (Fig. 12). Furthermore, Hp-1 to Hp-17 in Fig. 9 emblematized H_p signal at certain cycles ranging from 7800 cycles to 40000 cycles as shown as in Cycles row in Table 6. It is clearly shown in Fig. 9 that the H_p value increased dramatically at L_x 20 mm or at the SCZ area. Also, it can be seen that the SMFL signal patterns were very different between the elastic region and the pre-crack region. The H_p distribution for the values for sensor 1 ranged from -22 A/mm to -11 A/mm as tabulated in Table 6. This state occurred because sensor 1 had been scanned above the crack propagation and it was clearly demonstrated that the H_p value changed from the earlier state. Also, the grains and domain wall on the crack propagation region of the fracture were torn at the

Table 6 H_p values in the crack propagation region for sensor 1

Cycles	7,800	14,500	20,500	25,000	29,000	32,500	35,500	38,000	40,000
Crack length, mm	0	1	2	3	4	5	6	7	8
H_p at SCZ, A/mm	-22	-27	-27	-24	-21	-19	-18	-12	-11

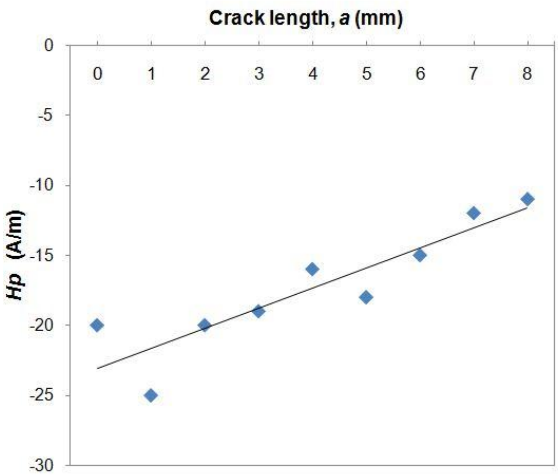

Fig. 10 Amplitude, H_p of a SMFL signal in the crack propagation region at crack starter notch for Sensor 1

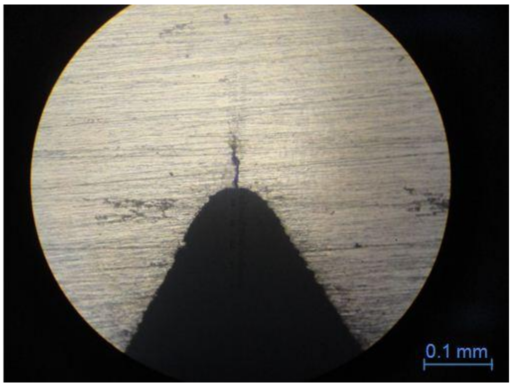

Fig. 11 25x microscopic image of the specimen surface when the crack started at 7,800 cycles

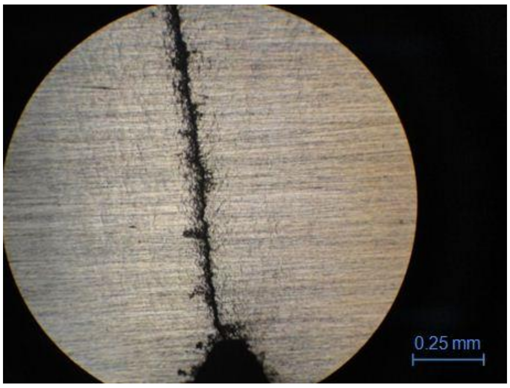

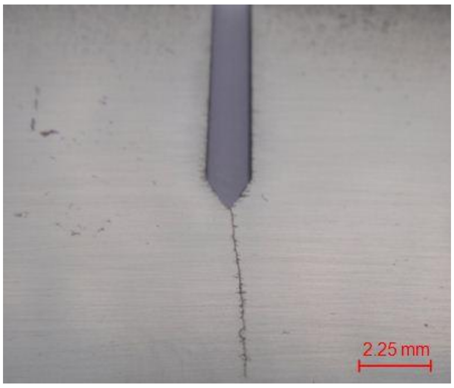

(a) (b)

Fig. 12 Micopic image of the specimen surface when the crack ended at 40,000 cycles, and the images were magnified (a) 10x; and (b) 1x

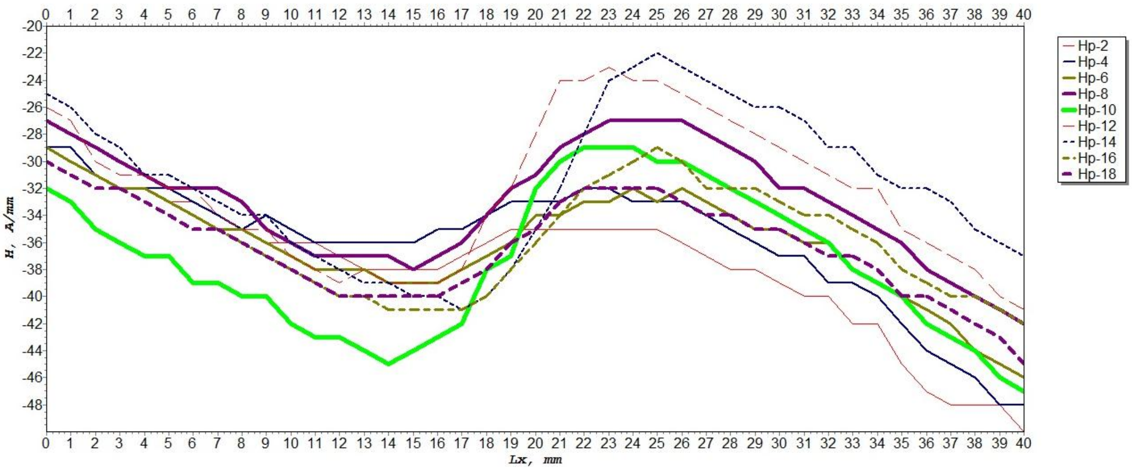

Fig. 13 Amplitude, H_p of SMFL signals in the crack propagation region for sensor 2

Table 7 H_p values in the crack propagation region for sensor 2

Cycles	7,800	14,500	20,500	25,000	29,000	32,500	35,500	38,000	40,000
Crack length, mm	0	1	2	3	4	5	6	7	8
H_p at SCZ, A/mm	-33	-31	-32	-31	-32	-31	-34	-36	-36

instant of failure. Furthermore, a discontinuity of magnetism in the specimen occurred when the generated fatigue crack formed a flaw with two cracked surfaces. Therefore, some magnetic flux leaked out into the air and caused this phenomenon. As a result, H_p value tends to increasing due to greater length of crack, as shown in Fig. 10. Moreover, this was resulted from surge of magnetic intensities due to crack propagation.

Fig. 13 represents the SMFL signals at the crack propagation region for sensor 2 and the H_p value at the SCZ range from -31 A/mm to -36 A/mm as in Table 7. Furthermore, Hp-2 to Hp-18 in Fig. 13 emblematized H_p signal at certain cycles ranging from 7800 cycles to 40000 cycles as shown as in Cycles row in Table 7. The signal patterns were similar to the plots in Fig. 7, which were in the pre-crack region. However, the H_p range of values were slightly lower due to a small dislocation in the microstructure causing lower magnetism during this condition. It can be explained that sensor 2 detected a similar signal condition as sensor 1 in the pre-crack region.

The gradient of H_p or dH/dx was also one of the criteria in the discussion about the SMLF criterion. Fig. 14 represents dH/dx from 7800 cycles - 40000 cycles, which are presented as Hp-1 to Hp-18 at the Channels axis, also, odd numbers represent for sensor 1 and even numbers

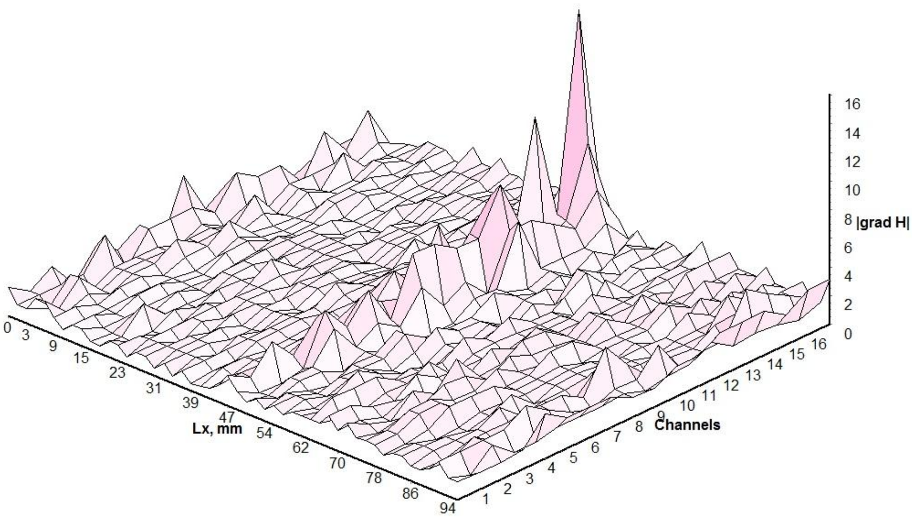

(a)

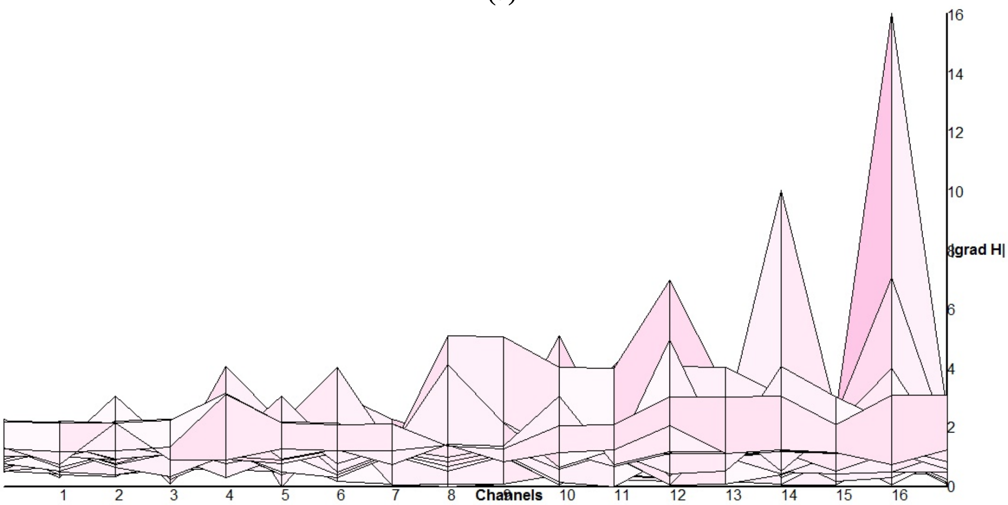

(b)

Fig. 14 H_p gradient of the SMLF: (a) contour view; (b) 2-dimensional view represent for sensor 2. The intensity of dH/dx was increasing from the starting point in the crack propagation region until the end of the experiment. It occurred at the area of L_x 20 mm or at the SCZ. This phenomenon resulted from changes in the microstructure of the specimen material and it tended to change the magnetic characteristics of the specimen. The microstructure of the material in the elastic region and the pre-crack region were different, but they were still in an almost solid state due to few dislocations. However, during the crack propagation, the microstructures were collapsing due to the cracking condition (Leng *et al*. 2009) and the increasing intensity of dH/dx.

5. Conclusions

Fatigue characterization using Metal Magnetic Memory in this study was successfully performed. The MMM device used along the specified scanning paths effectively detected the fatigue characteristics of the test specimen. This study demonstrated the applicability of MMM in detecting crack initiation and propagation on fatigue loading. Three conditions have been observed; the elastic, pre-crack and crack propagation regions. During the elastic region, the small decreasing value of H_p occurred due to few dislocations in the microstructure, while in the pre-crack region, more dislocations occurred that tended to lower the value of the H_p.

In the crack propagation region, the H_p values were increasing towards the zero value due to the occurrence of a discontinuity of magnetism in the specimen when the generated fatigue crack formed a flaw with two cracked surfaces. These result comparable to L. Dong finding, where, H_p increasing with increment of crack length (Dong *et al*. 2008). Also, this phenomenon resulted in an increase in the intensity of dH/dx. Moreover, an obvious change in dH/dx occurred at more than 20,500 cycles with a crack length 2 mm and it started increasing until the end of the experiment at 8 mm of crack length at 40,000 cycles. This resulted from the grains and domain wall on the crack propagation region of the fracture being torn due to the leakage of magnetic flux into the air. The study has also demonstrated that Metal Magnetic Memory is able to the detection of the fatigue characteristics of the material chosen. However, many things need to be researched such as the relationship between MMM with thickness of the material, the type of material, environment effect, etc., before MMM could be widely applied. This work is the first known attempt to correlate the MMM signal and also the crack growth propagation parameters by means of the increment of a specified crack length.

Acknowledgments

The authors would like to express their gratitude to Universiti Kebangsaan Malaysia and Ministry of Education (Malaysia) through the fund of FRGS/1/2012/TK01/UKM/03/2, for supporting this research.

References

C33, A. (2004), Standard Specification for Concrete Aggregates; ASTM International, West Conshohocken, PA, USA.

Changliang, S., Shiyun, D., Binshi, X. and Peng, H. (2010), "Stress concentration degree affects spontaneous magnetic signals of ferromagnetic steel under dynamic tension load", *NDT & E International*,

43(1), 8-12.

Dong, L., Xu, B., Dong, S., Chen, Q. and Dan, W. (2008), "Monitoring fatigue crack propagation of ferromagnetic materials with spontaneous abnormal magnetic signals", *Int. J. Fatig.*, **30**(9), 1599-1605.

Dong, L., Xu, B., Dong, S., Song, L., Chen, Q. and Wang, D. (2009), "Stress dependence of the spontaneous stray field signals of ferromagnetic steel", *NDT & E International*, **42**(4), 323-327.

Dong, L., Xu, B., Dong, S. and Chen, Q. (2010), "Characterisation of stress concentration of ferromagnetic materials by metal magnetic memory testing", *Nondestruct. Test. Eva.*, **25**(2), 145-151.

Dong, L.H., Xu, B.S., Wang, H.P. and Xue, N. (2012), "A physical model for self-emitting magnetic Signals during fatigue crack propagation", *Appl. Mech. Mater.*, **190-191**, 415-418.

Dubov, A.A. (1995), "Diagnostics of boiler tubes with usage of metal magnetic memory", *Moscow*: *Energoatomizdat*.

Dubov, A. (2006), "Principle features of metal magnetic memory method and inspection tools as compared to known magnetic NDT methods", *Can. Inst. Non-Destruct. Eva.* (*CINDE*) *J.*, **27**(3), 16.

Dubov, A. and Kolokolnikov, S. (2013), "The metal magnetic memory method application for online monitoring of damage development in steel pipes and welded joints specimens", *Welding in the World*, **57**(1), 123-136.

International, A. and Materials, A.S. for T.&. (2004), "Annual book of ASTM Standards", American Society for Testing & Materials.

Jiles, D. (1998), *Introduction to Magnetism and Magnetic Materials*, CRC Press.

Leng, J., Xu, M., Zhao, S. and Zhang, J. (2009), "Fatigue damage evaluation on ferromagnetic materials using magnetic memory method", *Proceedings of 2009 International Conference on Measuring Technology and Mechatronics Automation*, pp. 784-786.

Li, J. and Xu, M. (2012), "Influence of uniaxial plastic deformation on surface magnetic field in steel", *Meccanica*, **47**(1), 135-139.

Li, J.W., Xu, M.Q., Leng, J.C. and Xu, M.X. (2010), "The characteristics of the magnetic memory signals under different states for Q235 defect samples", *Adv. Mater. Res.*, **97-101**, 500-503.

Lindgren, M. and Lepistö, T. (2001), "Effect of prestraining on Barkhausen noise vs. stress relation", *NDT & E International*, **34**(5), 337-344.

Liu, C.K., Zhang, B., Chen, X., Ren, J.L., Tao, C.H. and He, Y.H. (2010), "Research on fatigue damage of ferromagnetic material by metal magnetic memory methods", *Adv. Mater. Res.*, **97-101**, 4501-4504.

Wang, Z.D., Yao, K., Deng, B. and Ding, K.Q. (2010a), "Quantitative study of metal magnetic memory signal versus local stress concentration", *NDT & E International*, **43**(6), 513-518.

Wang, Z.D., Yao, K., Deng, B. and Ding, K.Q. (2010b), "Theoretical studies of metal magnetic memory technique on magnetic flux leakage signals", *NDT & E International*, **43**(4), 354-359.

Wang, H.P., Dong, L.H., Dong, S.Y., Xue, N. and Xu, B.S. (2012), "Characterization of stress concentration degree based on 2-dementional magnetic memory signals", *Appl. Mech. Mater.*, **268-270**, 396-400.

Wang, Z.D., Gu, Y. and Wang, Y.S. (2012), "A review of three magnetic NDT technologies", *Journal of Magn. Magn. Mater.*, **324**(4), 382-388.

Xing, H.Y., Wu, D.B. and Xu, M.Q. (2010), "Material fatigue behavior and its mechanism based on MMM technology", *Adv. Mater. Res.*, **146-147**, 408-411.

Yang, L.J., Liu, B., Chen, L.J. and Gao, S.W. (2013), "The quantitative interpretation by measurement using the magnetic memory method (MMM)-based on density functional theory", *NDT & E International*, **55**, 15-20.

Yuan, J.J. and Zhang, W.M. (2011), "The surface weak magnetic signals of low carbon steel under cyclic loads", *Adv. Mater. Res.*, **298**, 197-202.

Zhang, Y.L., Gou, R.B., Li, J.M., Shen, G.T. and Zeng, Y.J. (2012), "Characteristics of metal magnetic memory signals of different steels in high cycle fatigue tests", *Fatigue Fract. Eng. Mater. Struct.*, **35**(7), 595-605.

CC